Magneto-optics in semiconductor crystals of arbitrary orientation

A. P. Roth and E. Fortin
Département de Physique, Université d'Ottawa, Ottawa, Canada
(Received 27 March 1978)

A model is developed for the interband magneto-optical transitions in zinc-blende structure semiconductors for the general case of arbitrary field orientation with respect to the crystal axis. This work is a generalization of the Pidgeon and Brown calculation for the special case of $\vec{B} \| (1\bar{1}0)$. Numerical calculations are performed for monocrystalline InSb, and the model is then adapted to the case of polycrystalline materials. Applications to interband magneto-optical results in polycrystalline InSb and $In_{0.58}Ga_{0.42}Sb$ are presented and discussed.

I. INTRODUCTION

Magneto-optical studies have long proved to be a very efficient method of determining band parameters in semiconductors. Work in this area, however, has dealt mainly with the case of monocrystalline materials: Not all materials are easy to obtain in single-crystal form, and interesting practical applications of polycrystals are now starting to appear, e.g., use in photovoltaic cells. In this paper we develop a general model for zinc-blende-structure semiconductor crystals in a magnetic field of arbitrary orientation, such a study being a prerequisite to the application of interband magneto-optics to the case of randomly oriented polycrystals.

The most realistic model for the quantization of electronic levels in a magnetic field, due to Pidgeon and Brown,[1] includes valence-band degeneracy and nonparabolicity of the conduction band and allows the calculation of the Landau-level energies in the particular case of monocrystals in a field oriented along the $(1\bar{1}0)$ plane. A method analogous to that in Ref. 1 is followed here to treat the general case of arbitrary field orientation. In Sec. II, the Hamiltonian matrix for the coupled valence and conduction bands is developed and the anisotropy of the Landau levels and valence-band effective masses are deduced. Numerical calculations are performed for InSb. In Sec. III we show how this anisotropy affects experimental interband transition spectra in polycrystals and we discuss an appropriate method of analysis for such experiments in connection with measurements on polycrystalline InSb and $In_{0.58}Ga_{0.42}Sb$ samples.

II. LANDAU LEVELS IN ZINC-BLENDE MONOCRYSTALS

A. Interaction matrix

In this section, we obtain the interaction matrix for zinc-blende monocrystals of arbitrary orientation with respect to the magnetic field direction. We follow a method analogous to that of Pidgeon and Brown[1] who restricted their calculations to a field directed along the $(1\bar{1}0)$ plane and we treat the conduction band (CB) together with the valence bands (VB) and split-off bands (SO) at Γ. As shown by Luttinger and Kohn,[2] the CB, VB, and SO energy levels are the eigenvalues of a set of eight coupled equations:

$$\sum_{j'} H_{jj'} f_{j'} = \epsilon f_j , \quad j, j' = 1, 8 , \tag{1}$$

where $H_{jj'}$ is the interaction matrix element between the states j and j'. The zero-order wave functions are written

$$\psi = \sum_j f_j u_{j0} , \tag{2}$$

where the u_{j0}'s are the band-edge wave functions. With the magnetic field orientation given by θ, ϕ with respect to the crystal axis (x, y, z), Eq. (1) can be written in the 1-2-3 reference system of Fig. 1 as follows:

$$\sum_{j'} \{ D^{\alpha\beta}_{jj'} k_\alpha k_\beta + \pi^\alpha_{jj'} k_\alpha + \tfrac{1}{2} s (\sigma_3)_{jj'} + (1/4c^2)[(\vec{\sigma} \times \nabla V) \cdot \vec{p}]_{jj'} + \epsilon_{j'} \delta_{jj'} \} f_{j'}(r) = \epsilon f_j(r) , \tag{3}$$

where

$$D^{\alpha\beta}_{jj'} = \tfrac{1}{2} \delta_{jj'} \delta_{\alpha\beta} + \sum_i \frac{\pi^\alpha_{ji} \pi^\beta_{ij'}}{\epsilon'_0 - \epsilon_i} , \tag{4}$$

and

$$\pi_{jj'} = \langle u_{j0}(r) | \vec{p} - (1/4c^2)(\nabla V \times \vec{\sigma}) | u_{j'0}(r) \rangle . \tag{5}$$

j and j' run over the two conduction-band plus six valence-band and six split-off-band states, i runs over all other bands and α, β run over 1, 2, 3. We use the Landau gauge $A = H(2, 0, 0)$ and put $\hbar = 1$, $m_0 = 1$, $s = eH/c$, where m_0 is the

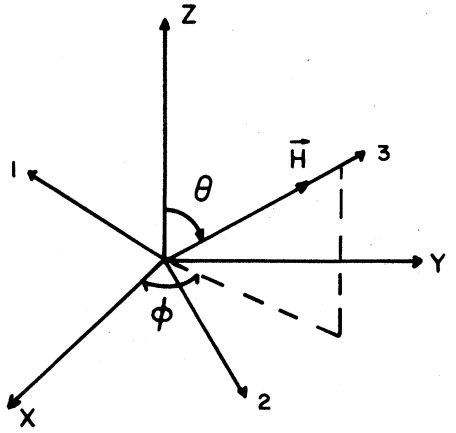

FIG. 1. Magnetic field orientation with respect to crystal axis (x, y, z); the 1-2-3 reference system is constructed with the field in the 3 direction.

free-electron mass and H the magnetic field. Following Kane[3] we neglect the second term in $\pi_{jj'}$. The band-edge wave functions are those which diagonalize the spin-orbit interaction:

$$
\begin{aligned}
&u_{10}=|S\uparrow\rangle', \quad u_{20}=|S\downarrow\rangle',\\
&u_{30}=|(1/\sqrt{2})(X+iY)\uparrow\rangle', \quad u_{40}=|(i/\sqrt{2})(X-iY)\downarrow\rangle',\\
&u_{50}=|(1/\sqrt{6})[(X-iY)\uparrow+2Z\downarrow]\rangle',\\
&u_{60}=|(i/\sqrt{6})[(X+iY)\downarrow-2Z\uparrow]\rangle',\\
&u_{70}=|(i/\sqrt{3})[-(X-iY)\uparrow+Z\downarrow]\rangle',\\
&u_{80}=|(1/\sqrt{3})[(X+iY)\downarrow+Z\uparrow]\rangle'.
\end{aligned}
\tag{6}
$$

u_{10} and u_{20} belong to Γ_6 and transform like s-type functions under T_d; u_{40}, u_{50}, u_{60}, u_{30} belong to Γ_8 and transform like p-type functions: They correspond to the $J=\frac{3}{2}$ set; u_{70} and u_{80} belong to Γ_7 and correspond to the $J=\frac{1}{2}$ set of p-type functions. Spin up and down are labeled by $\uparrow$ and $\downarrow$, and the prime indicates that the above functions are defined with respect to the 1-2-3 coordinate system.

Symmetry properties of the functions (6) are useful in the development of (3). We therefore write (3) and (6) in the x-y-z system. Transformation from one system to the other is performed using the rotation matrices:

$$
\begin{bmatrix} X' \\ Y' \\ Z' \end{bmatrix} = \begin{bmatrix} \cos\theta\cos\phi & \cos\theta\sin\phi & -\sin\theta \\ -\sin\phi & \cos\phi & 0 \\ \sin\theta\cos\phi & \sin\theta\sin\phi & \cos\theta \end{bmatrix} \begin{bmatrix} X \\ Y \\ Z \end{bmatrix}, \tag{7}
$$

$$
\begin{bmatrix} \uparrow' \\ \downarrow' \end{bmatrix} = \begin{bmatrix} e^{-i\phi/2}\cos\frac{1}{2}\theta & e^{i\phi/2}\sin\frac{1}{2}\theta \\ -e^{-i\phi/2}\sin\frac{1}{2}\theta & e^{i\phi/2}\cos\frac{1}{2}\theta \end{bmatrix} \begin{bmatrix} \uparrow \\ \downarrow \end{bmatrix}, \tag{8}
$$

and p_x, p_y, p_z also transform according to (7).

Once these transformations are carried out, the set of coupled equations can be written in a matrix form. (We put $k_3=0$ because we are interested in computing energies for optical transitions and the joint density of states for such transitions has a maximum for $k_3=0$.) In that case the 8×8 matrix reduces to two 4×4 matrices, each one corresponding to a set of 4 states, i.e., one conduction band plus two valence bands plus one split-off band. The two sets hereafter called a and b sets are decoupled and do not interact through a dipole interaction.

Each of these two matrices can in turn be written as the sum of two matrices, the second one being as a small perturbation on the first one. Symbolically,

$$
H^{88} = \begin{bmatrix} H_a^{44} & 0 \\ 0 & H_b^{44} \end{bmatrix}, \tag{9}
$$

$$
H^{44}=H_0^{44}+H_1^{44}; \tag{10}
$$

where $H_1^{44} \ll H_0^{44}$. u_{10}, u_{30}, u_{50}, u_{70} form the a set; u_{20}, u_{60}, u_{40}, u_{80} form the b set.

Table I gives the matrix elements $(H_{0a}^{44})_{jj'}$, $(H_{0b}^{44})_{jj'}$, and $(H_{1a}^{44})_{jj'}$. H_{1b}^{44} is similar to H_{1a}^{44}. F, P, Δ_0 are defined by Kane[3] and γ_1, γ_2, γ_3, κ are the modified Luttinger parameters[1] which can be expressed in term of A, B, C, D as defined by Kane.[3] E_0 is the energy gap at Γ at zero magnetic field, Δ_0 is the spin-orbit splitting of the valence bands and the other parameters defined above represent interband interactions. $\alpha^\dagger$ and α are creation and annihilation operators defined by

$$
\begin{aligned}
&\alpha^\dagger=(1/\sqrt{2s})(k_1+ik_2),\\
&\alpha=(1/\sqrt{2s})(k_1-ik_2),
\end{aligned}
\tag{11}
$$

and $N=\alpha^\dagger\alpha$. Table II gives the angular functions which appear in the matrix elements. We have neglected matrix elements containing the term G defined by Kane[3] because they have very little effect on the energy levels.[1]

As expected, these general matrices, valid for all orientations, reduce to the particular case calculated by Pidgeon and Brown[1,15] when $\phi=\frac{1}{4}\pi$ [i.e., with field in the $(1\bar{1}0)$ plane]. Neglecting the small perturbations H_{1a}^{44} and H_{1b}^{44}, which represent inversion asymmetry terms responsible only for weak interband transitions,[4] Eq. (3) is written in matrix form as follows:

$$
(H_{0a}^{44}-E_aI^{44})f_a=0; \quad (H_{0b}^{44}-E_bI^{44})f_b=0, \tag{12}
$$

where

$$
f_a=\begin{bmatrix} f_1 \\ f_3 \\ f_5 \\ f_7 \end{bmatrix} \quad \text{and} \quad f_b=\begin{bmatrix} f_2 \\ f_6 \\ f_4 \\ f_8 \end{bmatrix}. \tag{13}
$$

TABLE I. Interaction matrix elements for Landau levels in the conduction and valence bands at Γ in zinc-blende-type crystals in a magnetic field of arbitrary orientation (θ,ϕ) with respect to the crystal axis.

(j,j')	H^{44}_{0a}	H^{44}_{0b}	
(1,1)	$E_0+2sF(N+\frac{1}{2})+s(N+1)$	$E_0+2sF(N+\frac{1}{2})+sN$	(2,2)
(1,3)	$is^{1/2}P\alpha^\dagger$	$i(\frac{1}{3}s)^{1/2}P\alpha^\dagger$	(2,6)
(1,5)	$i(\frac{1}{3}s)^{1/2}P\alpha$	$is^{1/2}P\alpha$	(2,4)
(1,7)	$(\frac{2}{3}s)^{1/2}P\alpha$	$(\frac{2}{3}s)^{1/2}P\alpha^\dagger$	(2,8)
(3,3)	$-s[(\gamma_1+\gamma_{\theta'\phi})(N+\frac{1}{2})+\frac{3}{2}\kappa]$	$-s[(\gamma_1-\gamma_{\theta'\phi})(N+\frac{1}{2})+\frac{1}{2}\kappa]$	(6,6)
(3,5)	$-s\sqrt{3}\,\gamma_{\theta'\phi}\alpha^2$	$-s\sqrt{3}\,\gamma_{\theta'\phi}\alpha^2$	(6,4)
(3,7)	$is\sqrt{6}\,\gamma_{\theta'\phi}\alpha^2$	$is\sqrt{2}[\gamma_{\theta'\phi}(N+\frac{1}{2}+\frac{1}{2}(\kappa+1)]$	(6,8)
(5,5)	$-s[(\gamma_1-\gamma_{\theta'\phi})(N+\frac{1}{2})-\frac{1}{2}\kappa]$	$-s[(\gamma_1+\gamma_{\theta'\phi})(N+\frac{1}{2})-\frac{3}{2}\kappa]$	(4,4)
(5,7)	$is\sqrt{2}[\gamma_{\theta'\phi}(N+\frac{1}{2})-\frac{1}{2}(\kappa+1)]$	$is\sqrt{6}\,\gamma_{\theta'\phi}\alpha^{\dagger 2}$	(4,8)
(7,7)	$-s[\gamma_1(N+\frac{1}{2})-(\kappa+\frac{1}{2})]-\Delta_0$	$-s[\gamma_1(N+\frac{1}{2}+(\kappa+\frac{1}{2})]-\Delta_0$	(8,8)

H^{44}_{1a}

$$(1,1)=(1,3)=(1,5)=(1,7)=(7,7)=0$$

$$(3,3)=-s\left(\frac{\alpha^2+\alpha^{\dagger 2}}{2}g(\theta,\phi)+3\mathrm{Im}\,\alpha^{\dagger 2}h(\theta,\phi)\right)(\gamma_2-\gamma_3)=(5,5)$$

$$(3,5)=-sU(\gamma_2-\gamma_3);\quad (3,7)=is\sqrt{2}\,U(\gamma_2-\gamma_3)$$

$$(5,7)=-is\sqrt{2}\left[g(\theta,\phi)\left(\frac{\alpha^2+\alpha^{\dagger 2}}{2}\right)+3il(\theta,\phi)\left(\frac{\alpha^{\dagger 2}-\alpha^2}{2}\right)\right](\gamma_2-\gamma_3)$$

$$U=\alpha^{\dagger 2}[m(\theta,\phi)-\tfrac{1}{3}f(\theta,\phi)]-\tfrac{2}{3}[g(\theta,\phi)+3il(\theta,\phi)](N+\tfrac{1}{2})$$
$$-i\left(l(\theta,\phi)+\frac{h(\theta,\phi)}{\cos\theta}\right)(\alpha^{\dagger 2}-\alpha^2)$$

The f_i's are proportional to harmonic oscillator functions[5] and by inspection one can see that solutions of (12) are

$$\begin{aligned} &f_1=a_1\Phi_n,\quad f_2=a_2\Phi_n,\\ &f_3=a_3\Phi_{n-1},\quad f_6=a_6\Phi_{n-1},\\ &f_5=a_5\Phi_{n+1},\quad f_4=a_4\Phi_{n+1},\\ &f_7=a_7\Phi_{n+1},\quad f_8=a_8\Phi_{n-1}, \end{aligned} \tag{14}$$

TABLE II. Angular functions describing the Landau-level anisotropy at Γ.

$$\gamma_{\theta'\phi}=\gamma_3+(\gamma_3-\gamma_2)f(\theta,\phi)$$
$$\gamma_{\theta'\phi}=\tfrac{1}{3}\gamma_2+\tfrac{2}{3}\gamma_3+\tfrac{1}{6}(\gamma_3-\gamma_2)f(\theta,\phi)$$
$$f(\theta,\phi)=\tfrac{3}{4}\sin^2\theta[\cos^2\theta(4-\sin^2 2\phi)+\sin^2 2\phi]-1$$
$$g(\theta,\phi)=\tfrac{3}{4}\sin^2\theta[\cos^2\theta(4-\sin^2 2\phi)-\sin^2 2\phi]$$
$$h(\theta,\phi)=\tfrac{1}{4}\sin 4\phi\sin^2 2\theta\cos\theta$$
$$l(\theta,\phi)=\tfrac{1}{4}\sin 4\phi(\sin^2\theta-2)\cos\theta$$
$$m(\theta,\phi)=2(\tfrac{1}{3}+\cos^2\theta\sin^2 2\phi)$$

where the Φ_n's are the harmonic-oscillator functions mentioned above. Substituting (14) into (12), the two matrices can be diagonalized numerically for a given set of band parameters and for any direction of the magnetic field.

B. Anisotropy of the Landau levels and of the effective masses

Since no exact analytical solution of (12) can be derived for any field direction, numerical diagonalization of H^{44} must be performed in order to study the effect of field orientation on the Landau levels. As an example, we have diagonalized H^{44}_{0a} and H^{44}_{0b} for InSb using published values of the band parameters.[1,16] The calculations were performed for different magnetic field intensities and directions. Some typical results are presented in Figs. 2–5 for $B=3$ T; the general features would be similar for different field values and for other III-V compounds.

In Fig. 2(a) we have plotted the first Landau levels of the a set for a particular field intensity ($B=3$ T) and orientation ($\theta=0$, $\phi=0$), i.e., the [100] direction. One can note the irregular spac-

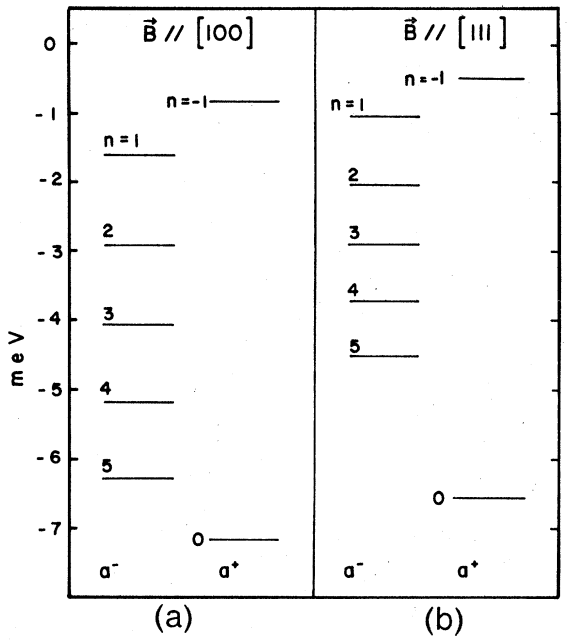

FIG. 2. (a) Valence-band levels (a set) for InSb with $\vec{B} \parallel [100]$, $B = 3$ T. (b) Valence-band levels (a set) for InSb with $\vec{B} \parallel [111]$, $B = 3$ T. The numerical values were calculated from the diagonalization of H_{0a}^{44} and H_{0b}^{44} with published values of band parameters (Refs. 1 and 16).

ing of the levels which is caused by the degeneracy at Γ. This appears for all θ and ϕ, but the spacing between two levels n and n', is different for different θ and ϕ as can be seen by comparing Fig. 2(a) with 2(b), where we have plotted the same levels for $\theta = 54.7°$ and $\phi = 45°$ (i.e., the [111] direction). Only the a set is considered here for simplicity. The variation of a given energy level with field orientation can be obtained as well and we show in Fig. 3 such a variation for the $n = 3$ level of the a set, calculated for $B = 3$ T. The different energy variation of the conduction-band and valence-band levels can be qualitatively explained with the help of approximate equations. The determinantal equation (12) can be developed and gives terms up to fourth order in the magnetic field. One can expand the solutions in a power series in s

$$E = E^{(0)} + E^{(1)}s + E^{(2)}s^2 + E^{(3)}s^3 + \cdots . \tag{15}$$

Substituting this expansion into the determinantal equation and grouping terms containing equal powers of s allows one to obtain $E^{(0)}, E^{(1)}, E^{(2)}, \ldots$ for each band. The procedure is straightforward but yields very complicated expressions except for the first coefficients. The a-set conduction-band levels, the heavy- and light-hole levels are then given by

$$E_c^{\alpha} = E_0 + \left\{ \left(n + \tfrac{1}{2}\right) \left[1 + 2F + \frac{E_p}{3}\left(\frac{2}{E_0} + \frac{1}{E_0 + \Delta_0}\right)\right] + \frac{1}{2}\left[1 - \frac{E_p}{3}\left(\frac{1}{E_0} - \frac{1}{E_0 + \Delta_0}\right)\right]\right\} s + E_c^{(2)}(\theta, \phi)s^2 + \cdots , \tag{16}$$

$$E_{\rm hh}^{a^-} = -\left([(n - \tfrac{3}{2})\gamma_1^L - \gamma_{\theta\phi}'^L + \tfrac{1}{2}\kappa^L] + \{[\gamma_1^L - (n - \tfrac{3}{2})\gamma'^L - \kappa^L]^2 + 3n(n+1)(\gamma_{\theta\phi}''^L)^2\}^{1/2}\right) s + E_{\rm hh}^{a(2)}(\theta, \phi)s^2 + \cdots , \tag{17}$$

$$E_{\rm lh}^{a^+} = -\left([(n - \tfrac{3}{2})\gamma_1^L - \gamma_{\theta\phi}'^L + \tfrac{1}{2}\kappa^L] - \{[\gamma_1^L - (n - \tfrac{3}{2})\gamma_{\theta\phi}'^L - \kappa^L]^2 + 3n(n+1)(\gamma_{\theta\phi}''^L)^2\}^{1/2}\right) s + E_{\rm lh}^{a(2)}(\theta, \phi)s^2 + \cdots , \tag{18}$$

where

$$\begin{aligned} \gamma_1^L &= \gamma_1 + E_p/3E_0 , \\ \gamma_{\theta\phi}'^L &= \gamma_{\theta\phi}' + E_p/6E_0 , \\ \gamma_{\theta\phi}''^L &= \gamma_{\theta\phi}'' + E_p/6E_0 , \\ \kappa^L &= \kappa + E_p/6E_0 , \\ E_p &= 2mP^2/\hbar^2 . \end{aligned} \tag{19}$$

Similar equations can be obtained for the split-off band and the b-set levels. $E_c^{(2)}(\theta, \phi)$ is a combination of all H_{0a}^{44} matrix elements and depends on (θ, ϕ) through $\gamma_{\theta\phi}'$ and $\gamma_{\theta\phi}''$. Comparing (16) and (17) we see that the angular dependence of the conduction-band levels appears in the s^2 coefficient while the s coefficient of the heavy-hole levels development depends strongly on field orientation through $\gamma_{\theta\phi}'$ and $\gamma_{\theta\phi}''$. The s coefficient of the light-hole levels consists of the difference between two terms, and thus these levels exhibit a smaller variation than the heavy-hole levels. Maximum relative variation of the three levels presented in Fig. 3 are approximately

$$\begin{aligned} \frac{\Delta E_c^{\alpha}}{\frac{1}{2}|E_{c[100]}^{\alpha} + E_{c[111]}^{\alpha}|} &= \pm 0.02\% , \\ \frac{\Delta E_{\rm hh}^{a^-}}{\frac{1}{2}|E_{\rm hh[100]}^{a^-} + E_{\rm hh[111]}^{a^-}|} &= \pm 17\% , \\ \frac{\Delta E_{\rm lh}^{a^+}}{\frac{1}{2}|E_{\rm lh[100]}^{a^+} + E_{\rm lh[111]}^{a^+}|} &= \pm 0.2\% . \end{aligned} \tag{20}$$

The anisotropy of the hole masses is shown in Figs. 4 and 5. Approximate equations for the hole anisotropy can be obtained from the developments (17) and (18)

$$\begin{aligned} m_{\rm hh}/m &= \{\gamma_1^L - [(\gamma_{\theta\phi}'^L)^2 + 3(\gamma_{\theta\phi}''^L)^2]^{1/2}\}^{-1} , \\ m_{\rm lh}/m &= \{\gamma_1^L + [(\gamma_{\theta\phi}'^L)^2 + 3(\gamma_{\theta\phi}''^L)^2]^{1/2}\}^{-1} . \end{aligned} \tag{21}$$

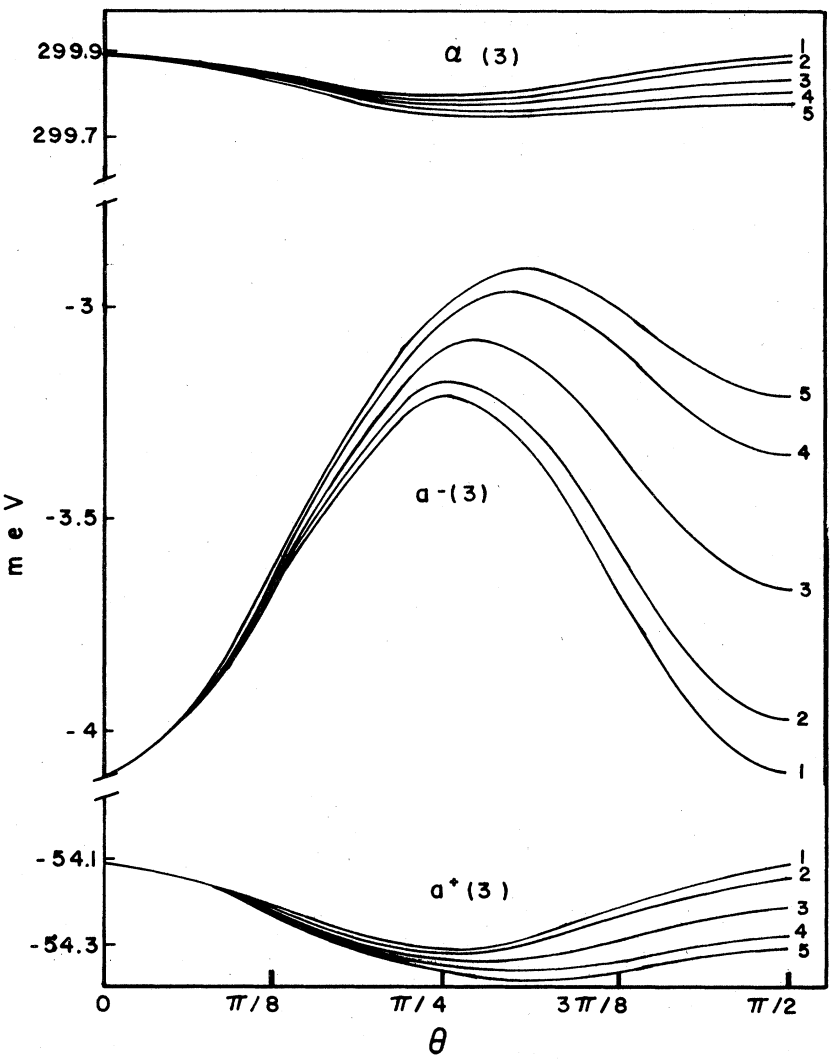

FIG. 3. Anisotropy of the $n=3$ levels (α set) in the conduction band (α), heavy-hole (α^-), and light-hole (α^+) valence bands. Curves 1–5 correspond to $\phi=0$, $\pi/16$, $\pi/8$, $3\pi/16$, and $\pi/4$, respectively.

Relative variations of the hole masses for InSb are deduced from the graphs of Figs. 4 and 5:

$$\frac{\Delta m_{\mathrm{hh}}}{\frac{1}{2}\left|m_{\mathrm{hh}[100]}+m_{\mathrm{hh}[111]}\right|}=\pm 16\%\,,$$

$$\frac{\Delta m_{\mathrm{lh}}}{\frac{1}{2}\left|m_{\mathrm{lh}[100]}+m_{\mathrm{lh}[111]}\right|}=\pm 0.7\%\,. \tag{22}$$

The small variation of the light-hole mass explains why experimental values are usually given as isotropic.

C. Application to interband transitions in monocrystals

The Landau-level anisotropy has an important effect on interband magneto-optical experiments. As we show in Fig. 6 for absorption, a given transition (fixed n, n') will occur at different energies for different field orientations. We have restricted this figure to heavy-hole transitions which are the more intense, with $\Delta n=-1$ and B parallel to [100] and [111]. These two directions give the maximum energy difference for a given index. Values of ΔE, the energy difference illustrated in Fig. 6, calculated for different n and B values, for InSb and GaSb are shown in Table III. The last column gives an estimated precision easily achieved experimentally at these transition energies. This table has been obtained by numerical diagonalization of the interaction matrices H_{0a}^{44} and H_{0b}^{44} of Table I with published values of the band parameters.[1,6] In most cases the energy difference is measurable under normal experimental conditions. The effects of H_{1a}^{44} and H_{1b}^{44} can be introduced by means of second-order perturbation theory[1] to study weak transitions.

The generalization of Pidgeon and Brown's method to arbitrary field orientation described in this section can thus be used for monocrystals

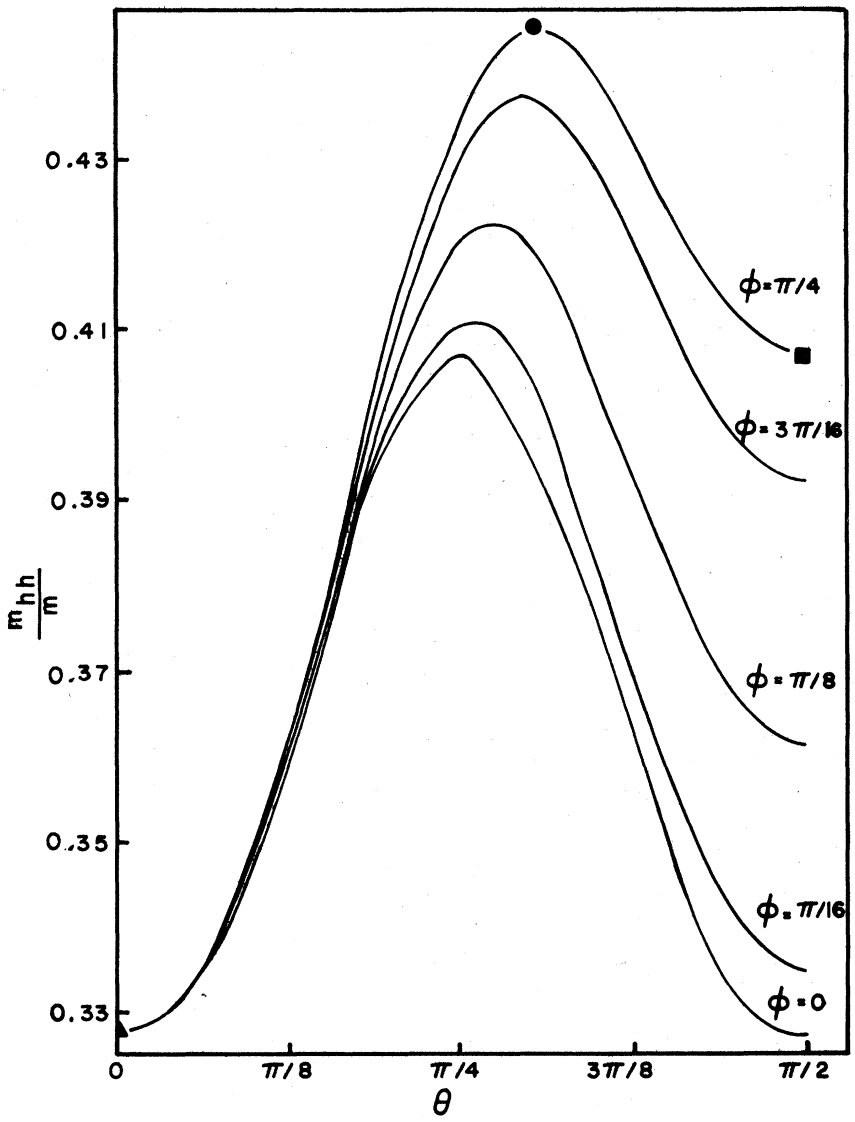

FIG. 4. Anisotropy of the heavy-hole mass at Γ in InSb. The main crystallographic direction values are indicated by: ▲[100], ●[110], ■[111].

but can also be adapted to the study of polycrystals as discussed in Sec. III.

III. APPLICATION TO POLYCRYSTALS

A. Broadening of oscillations in interband magneto-absorption experiments

The general model developed in Sec. II can be used to interpret experimental results obtained with polycrystalline materials. Consider, for instance, a sample made of small crystallites randomly oriented in a magnetic field of given direction. Due to anisotropy, the Landau-level pattern will be different for crystallites of different orientations. Under proper illumination, interband transitions will take place in each crystallite and transitions involving the same indices (n,n') will have different energies for different orientations of the crystallites. Furthermore the energy spacing between transitions in a single crystallite varies with (n,n') and this variation depends on orientation as was shown in Sec. II.

The two phenomena—anisotropy of each transition and variable energy spacing between transitions—will thus combine to give an experimental magneto-absorption spectrum with broader oscillations and fewer observable transitions than that of a monocrystal. This can be easily visualized if the experimental absorption curve is considered as the sum of individual absorption curves arising from each crystallite. Each individual spectrum would show oscillating structures with variable spacing of the oscillations and this spacing would vary in

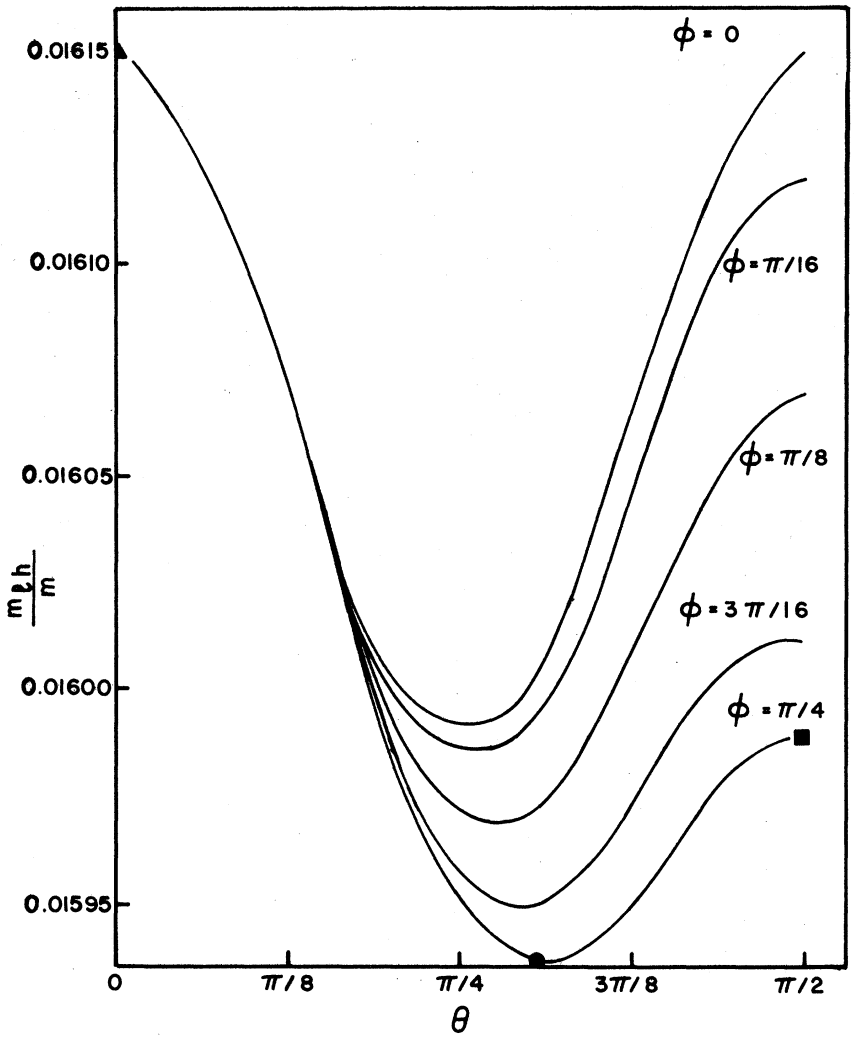

FIG. 5. Anisotropy of the light-hole mass at Γ in InSb. The values for the main crystallographic direction are indicated by ▲[100], ●[110], ■[111].

TABLE III. Energy difference of some heavy-hole interband transitions in InSb and GaSb for $\vec{B}$ || [100] and $\vec{B}$ || [111]. $a^-(n)$, $\alpha(n)$ refer to heavy-hole and conduction-band levels of the a set; $b^-(n)$, $\beta(n)$ refer to the b set. These values have been obtained from the diagonalization of H^{44}_{0a} and H^{44}_{0b} with published values of the band parameters (Refs. 1 and 6).

Material	Transition [a]	$\Delta E = E_{[100]} - E_{[111]}$ (meV) 3 T	5 T	7 T	Experimental precision (meV)
InSb	$H(2,1)$	0.7	1.2	1.8	0.5 to 0.7
	$H(1,2)$	0.5	0.8	1.2	
	$H(3,2)$	1.1	1.9	2.7	
	$H(2,3)$	0.9	1.6	2.3	
	$H(4,3)$	1.5	2.5	3.6	
GaSb	$H(2,1)$	0.8	1.3	1.9	0.7 to 1.0
	$H(1,2)$	0.5	0.7	1.1	
	$H(3,2)$	1.2	2.0	2.8	
	$H(2,3)$	0.8	1.5	2.1	
	$H(4,3)$	1.4	2.7	3.8	

[a] $H(n,n') = \frac{1}{2}\{[a^-(n) \rightarrow \alpha(n')] + [b^-(n) \rightarrow \beta(n')]\}$. Notation of Ref. 1.

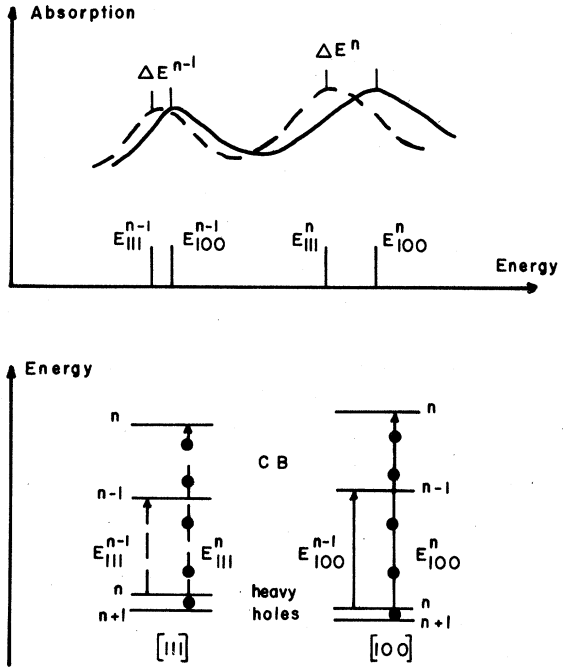

FIG. 6. Energy difference of heavy-hole interband transitions for $\vec{B}\|[100]$ and $\vec{B}\|[111]$. Only $\Delta n=-1$ transitions are considered for clarity.

a different manner for different orientations according to the general features discussed in Sec. II.

An additional source of oscillation broadening and of reduction in the number of observable transitions could be the lower relaxation time τ in a polycrystal as compared with that in a monocrystal: For two such samples, with the same impurity concentration, τ can be lower in the polycrystal due to the scattering at the crystallite boundaries. However, if crystallites are large enough for the condition $\omega\tau>1$ to be satisfied in each of them (i.e., the orbit size of the electrons is smaller than the crystallite size), then this scattering should have little effect in the broadening of the oscillations. Furthermore boundary scattering should affect all types of optical transitions even in the absence of a magnetic field; but experiments on III-V alloys[7] for instance, have shown no extra broadening when polycrystals were used instead of monocrystals. The Landau-level anisotropy can therefore be expected to be the main cause of oscillation broadening in interband magneto-optical spectra on polycrystals.

B. Analysis of the interband transitions

In the analysis of experimental data obtained by interband magneto-optical experiments, theoretical transition energies are fitted to experimental values. This fitting procedure is performed by a variation of band parameters. In a monocrystal, the orientation of the magnetic field is known, the angular functions [mainly $f(\theta,\phi)$] are calculated for the orientation and kept fixed, and the variable parameters are m_c, γ_1, γ_2, γ_3, P, F which are all orientation independent.

In the case of polycrystalline samples, the anisotropy problems can be handled by making use of various approximations. The experimental transition energies correspond to the average values of the transition energies arising from all crystallites. Theoretical average energies must be computed and the band parameters adjusted to minimize the deviation between theoretical and experimental values.

If the crystallites are uniformly oriented in a solid angle Ω, the actual theoretical average energy for each transition is

$$E_\Omega=\frac{1}{\Omega}\int_\Omega E(\theta,\phi)\,d\Omega\,.$$

As discussed in Sec. II, no exact analytical form for $E(\theta,\phi)$ can be obtained for an arbitrary direction and therefore E_Ω cannot be calculated exactly. Approximations can be introduced in the following ways. In a first method, one can choose a set of orientation-independent parameters and diagonalize the interaction matrices for several directions in the solid angle Ω to obtain transition energies for each of those directions. The averages of the numerical values thus obtained for each transition are then compared with the experimental data. If this sequence is performed with different sets of orientation-independent parameters, the best set of such parameters can be determined. In the limit where an infinite number of directions uniformly distributed in Ω is included in the calculation, the average energies obtained by this method for each transition are equal to the exact average energies defined above. The orientation-independent parameters determined in that case are identical with those of the corresponding monocrystal.

In a second method, one can define average Hamiltonian matrices $\overline{H}^{44}(\Omega)$ by using the angle-averaged values of the angular functions in Table II instead of the functions themselves. A best-fit procedure identical to the one used for monocrystals can then be carried out with these average matrices.

It must be noted that the average Hamiltonian retains all the basic features of the original matrices; in particular the valence-band anisotropy factor $(\gamma_3-\gamma_2)$ is still present. If the sample is made of a large number of crystallites oriented randomly in all directions, the solid angle Ω is 4π. In this case, the matrices of Table I take a simple form with

$$\bar{f}=-\tfrac{2}{5};\ \bar{g}=\tfrac{1}{10};\ \bar{h}=0;\ \bar{l}=0;\ \bar{m}=\tfrac{5}{6}. \qquad (23)$$

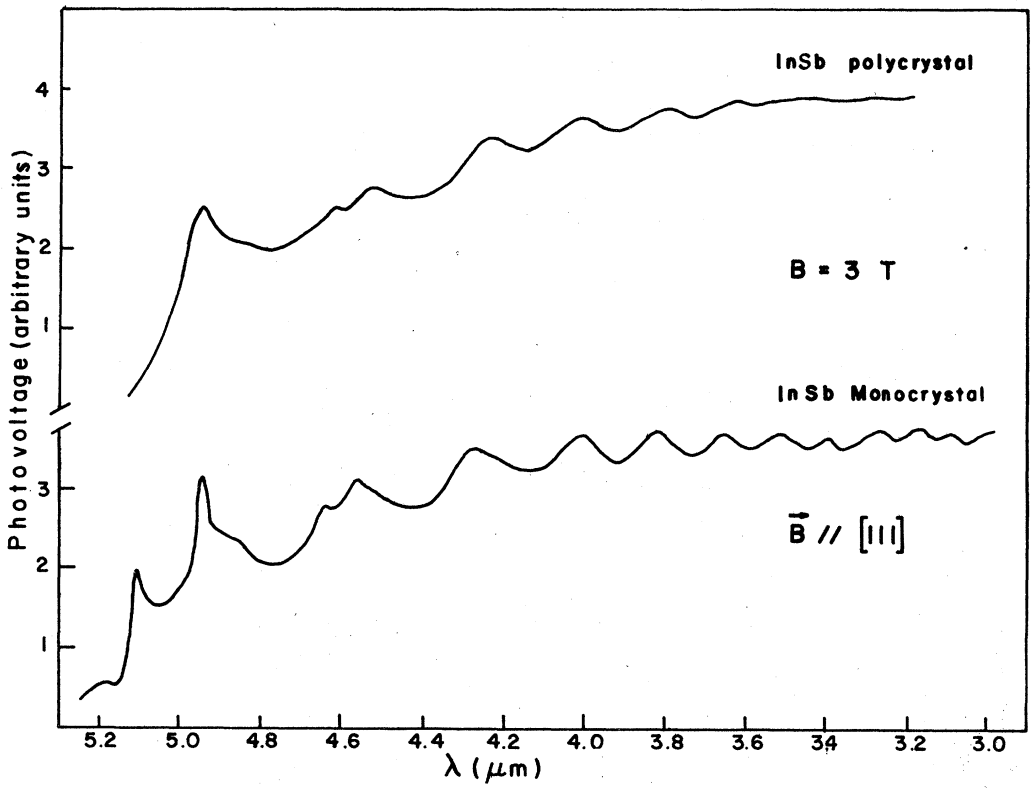

FIG. 7. Spectral variation of the photovoltage for InSb with $B = 3$ T. The upper curve corresponds to a polycrystalline sample, while the lower curve corresponds to a monocrystal and is taken from Ref. 11.

Substitution of $\bar{f}$ into $\gamma'_{\theta\phi}$ and $\gamma''_{\theta\phi}$ yields

$$\bar{\gamma}' = \bar{\gamma}'' = \tfrac{1}{5}(2\gamma_2 + 3\gamma_3) . \tag{24}$$

We have compared the average transition energies calculated by the two methods for InSb and GaSb. Calculations were made for B values up to 7 T and n values up to 20 for the case of heavy-hole transitions, which are the ones most affected by anisotropy. Provided enough orientations are included in the first method, the energy difference between the values obtained by the two approximations using the same set of orientation-independent parameters is much smaller than the usual experimental precision achieved in interband magneto-optics. For example, if we take more than 80 different directions with $\theta \in [0, \frac{1}{2}\pi]$ and $\phi \in [0, \frac{1}{4}\pi]$ in the first method, the energy difference for the $n = 10$ to $n' = 9$ a-set heavy-hole transition with $B = 3$ T is smaller than 0.2 meV in InSb and GaSb. When the number of directions included in the first method is increased the energy difference decreases. Therefore, the orientation-independent band parameters determined for InSb and GaSb by both methods are the same (within the experimental precision) and are identical with those of monocrystalline samples.

While the two methods are equivalent in accuracy, the second method is much faster in terms of computing time, and accordingly was used to analyze the results presented in Sec. III C.

C. Application to experimental results on InSb and $In_{0.58}Ga_{0.42}Sb$

The study of photovoltaic spectra has proved to be a successful method for collecting interband magneto-optical data in semiconductors, since such spectra are easily obtained and are directly related to absorption spectra.[8] Experiments of that type have been described in detail for monocrystalline samples of Ge,[9] InP,[10] and InSb.[11]

Polycrystals of InSb and $In_{0.58}Ga_{0.42}Sb$ were studied by this method. n-type InSb samples with $n = 10^{16}$ cm^{-3} and of typical dimensions $1 \times 3 \times 5$ mm^3 consisted of small crystallites, the size of which was estimated from x-ray back Laue photographs to be of the order of 0.1 mm in linear dimensions at the sample surface. After mechanical polishing and chemical etching, a thin gold film was deposited under vacuum on the front surface of the sample to build a Schottky barrier. Ohmic contacts on the back surface were made by vacuum

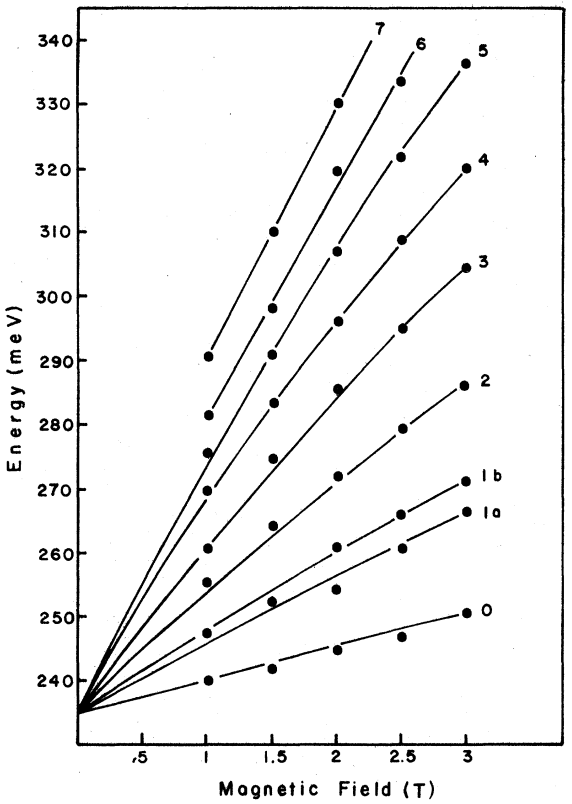

FIG. 8. Transition energies for polycrystalline InSb as functions of the magnetic field. The full lines are calculated values from the theory discussed in the text. Transitions are labelled according to Table IV.

deposition of indium. At room temperature the photosignal was small but increased at lower temperature in agreement with a model proposed recently.[8] All measurements were performed at 6 K in the Faraday configuration.

A typical spectrum of the photoresponse at $B = 3$ T is presented in Fig. 7 together with the result obtained with a monocrystal of InSb of comparable purity oriented with $\vec{B} \parallel [111]$ under the same experimental conditions.[11] The general features described in Sec. III A can be clearly seen in the spectrum of the polycrystal: Broadening and displacement of the oscillations, and a smaller number of observed transitions. The first structures are influenced by excitons[11]; no attempt was made, however, to apply the theory of Altarelli and Lipari[12,13] to interpret the displacement of the excitonic structures with magnetic field, because this theory is not directly applicable to polycrystals. Theoretical transition energies were calculated with averaged Hamiltonian matrices H_{0a}^{44} and H_{0b}^{44} and $\bar{f} = -\frac{2}{5}$ since the crystallites were randomly oriented. The best fit to the experimental values was achieved by

TABLE IV. Identification of the transitions observed in InSb and $In_{0.58}Ga_{0.42}Sb$ in the notation of Ref. 1.

Number	Transition [a]
0	$b^+(-1) \rightarrow \beta(0)$; $b^-(1) \rightarrow \beta(0)$
1a	$a^+(1) \rightarrow \alpha(0)$; $HH(2,1)$
1b	$a^+(0) \rightarrow \alpha(1)$; $b^+(0) \rightarrow \beta(1)$
$n \geq 2$	$HH(n+1, n-1, n)$

[a] $HH(n,n') = \frac{1}{2}\{[a^-(n) \rightarrow \alpha(n')] + [b^-(n) \rightarrow \beta(n')]\}$, $HH(n+1, n-1, n) = \frac{1}{2}[HH(n+1, n) + HH(n-1, n)]$. Notation of Ref. 1.

making use of only transitions having larger values of the indices ($n' \geq 2$), which are little influenced by excitons. Experimental points and theoretical curves are plotted in Fig. 8, and the transitions are identified in Table IV. Band parameters deduced from the analysis are compared with Pidgeon and Brown's values (which give the best fit for monocrystalline InSb[11]) in Table V. Heavy-hole effective masses in the main crystallographic directions are calculated from Eq. (21) and g_c is obtained from Eq. (16). All adjustable parameters were varied together to minimize the root-mean-square deviation between experimental and theoretical points. The uncertainty on each parameter is calculated from the maximum independent variation of that parameter which would increase the rms deviation by less than 1%. This uncertainty reflects the broadening of the oscillations in the experiments carried out on polycrystals. Taking into account these uncertainties, the overall agreement between the two sets is satisfactory. These results on InSb confirm that a unique set of band parameters can be obtained from experiments on single crystals or polycrystals as discussed above.

A similar experiment was performed on $In_{0.58}Ga_{0.42}Sb$. The sample was cut from a homogeneous polycrystalline ingot of $In_{1-x}Ga_xSb$ obtained by the step-freezing method.[14] Crystallite size varies with x in the ingots as could be seen from x-ray back Laue photographs. The sample with $n \simeq 6 \times 10^{15}$ cm^{-3} was made of randomly oriented crystallites smaller than those of the InSb samples used in the previous experiment. Magneto-optical data were obtained under the same experimental conditions as for InSb except that B values up to 7 T were used. The analysis was made following the method described above and theoretical transition energies are compared with experimental points in Fig. 9. The transitions are identified in Table IV and the band parameters for that particular material are given in the last column of Table V. It must be noted that the present results are the first measure-

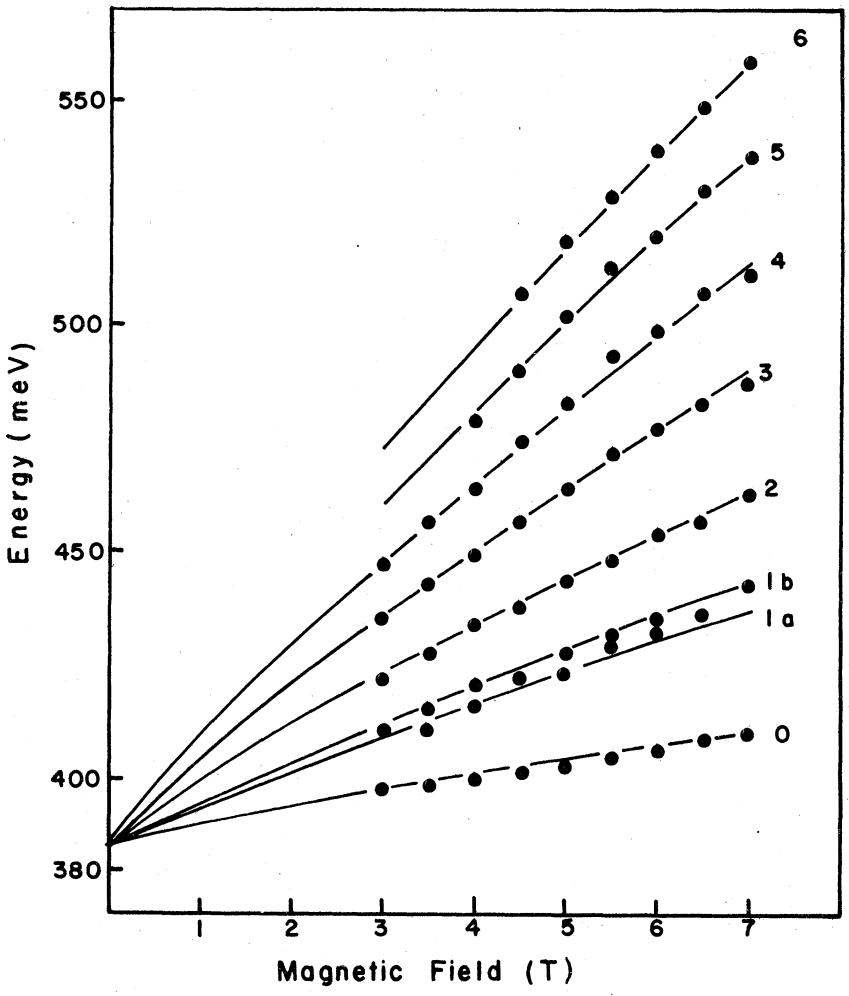

FIG. 9. Transition energies for polycrystalline $In_{0.58}Ga_{0.42}Sb$ as functions of the magnetic field. The full lines are the calculated values from the theory discussed in the text. Transitions are labelled according to Table IV.

ments on this alloy of all these band parameters at 6 K in a single experiment, thus yielding a consistent set of values. In both the InSb and $In_{0.58}Ga_{0.42}Sb$ experiments the precision of the measurements, and thus of the band parameters obtained could conceivably be enhanced by using differential techniques such as wavelength modulation,[10] or stress modulation[15] on the photovoltaic signal.

IV. CONCLUSION

The important effects of the Landau-level anisotropy in magneto-optics have been studied in this paper. The interaction matrices developed in Sec. II to calculate the energy levels in the conduction and valence bands of a monocrystal in a magnetic field oriented in any direction allow the determination of a unique set of band parameters, with their anisotropy at Γ, from the results of a single experiment. Furthermore, the model can easily be extended to the case of polycrystals and in addition explains partially the shape of the interband-absorption spectra in such materials, as shown for the specific example of InSb. The study of alloy-semiconductor materials which are difficult to obtain in monocrystalline form can benefit from the application of magneto-optical methods to the case of polycrystals. The sample studied here, $In_{0.58}Ga_{0.42}Sb$, gave encouraging results and the studies will be extended throughout the composition range of $In_{1-x}Ga_xSb$ and other alloys. The consistent set of parameters thus obtained should help in the construction of a theory which would explain satisfactorily the variation of band parameters in III-V alloys.

ACKNOWLEDGMENTS

The authors wish to thank J. C. Woolley, R. C. Smith, and K. S. Song for valuable discussions. This research was supported by the National Research Council of Canada, and by a fellowship (to A.P.R.) from the Canada Council.

TABLE V. Band parameters of InSb and $In_{0.58}Ga_{0.42}Sb$. Experimental values obtained in this work for InSb are compared with the best set of parameters obtained for monocrystalline InSb (Refs. 1, 11, and 16).

Band parameter	InSb This work (Polycrystal)	InSb Ref. 1 (Monocrystal)	$In_{0.58}Ga_{0.42}Sb$ (Polycrystal)
E_0 (eV)	0.235 ±0.001	0.2355	0.3860 ± 0.0015
Δ_0 (eV)	0.81 [a]	0.9	0.71 ±0.02
m_c/m_0	0.0145 ± 0.0001	0.0145	0.0228 ± 0.0001
γ_1^L	32.4 ±0.1	32.5	23.6 ±0.01
γ_2^L	14.3 ±0.1	14.3	9.8 ±0.1
γ_3^L	15.4 ±0.1	15.4	11.0 ±0.1
E_p (eV)	21.53 ±0.25	21.92	21.72 ±0.15
g_c	−45.4 ±0.2	−48	−22.3 ±0.5
$\overline{m_{lh}}/m_0$	0.0160 ± 0.0002	0.0160	0.0224 ± 0.0002
$\overline{m_{hh}}/m_0$	0.3876		0.4026
$m_{hh[100]}/m_0$	0.325	0.30	0.330
$m_{hh[111]}/m_0$	0.445	0.44	0.473
$m_{hh[110]}/m_0$	0.407	0.42	0.426
F	0 ±0.1	0	−0.63 ±0.1

[a] Reference 16.

[1] C. R. Pidgeon and R. N. Brown, Phys. Rev. 146, 575 (1966).
[2] J. M. Luttinger and W. Kohn, Phys. Rev. 97, 869 (1955).
[3] E. O. Kane, J. Phys. Chem. Solids 1, 249 (1957).
[4] C. R. Pidgeon and S. H. Groves, Phys. Rev. 186, 824 (1969).
[5] S. H. Groves, R. N. Brown, and C. R. Pidgeon, Phys. Rev. 161, 779 (1967).
[6] A. Filion and E. Fortin, Phys. Rev. B 8, 3852 (1973).
[7] O. Berolo, Ph.D. thesis (University of Ottawa, 1973) (unpublished).
[8] P. Rochon, E. Fortin, and J. C. Woolley, Can. J. Phys. 55, 1145 (1977).
[9] P. Rochon and E. Fortin, Can. J. Phys. 52, 1173 (1974).
[10] P. Rochon and E. Fortin, Phys. Rev. B 12, 5803 (1975).
[11] P. Rochon and E. Fortin, Phys. Rev. B 15, 2025 (1977).
[12] M. Altarelli and N. O. Lipari, Phys. Rev. B 7, 3798 (1973).
[13] M. Altarelli and N. O. Lipari, Phys. Rev. B 9, 1733 (1974).
[14] W. M. Coderre and J. C. Woolley, Can. J. Phys. 47, 2553 (1969).
[15] R. L. Aggarwal, in *Semiconductors and Semimetals*, edited by R. K. Willardson and A. C. Beer (Academic, New York, 1972), Vol. 9, p. 151.
[16] C. R. Pidgeon, S. H. Groves, and J. Feinleib, Solid State Commun. 5, 677 (1967).